Random phase-shifting interferometry without accurately controlling or calibrating the phase shifts

Qun Hao,* Qiudong Zhu, and Yao Hu

Opto-Electronic College, Beijing Institute of Technology, Beijing 100081, China
**Corresponding author: qhao@bit.edu.cn*

Received January 5, 2009; revised March 15, 2009; accepted March 23, 2009;
posted March 26, 2009 (Doc. ID 105897); published April 14, 2009

A random phase-shifting interferometry insensitive to environmental noises is proposed. The relationship between intensity and phase in each pixel is obtained from a large amount of phase-shifting interferograms. In the phase-solving algorithm, the phase shift step length is not taken as a parameter, but the temporal intensity maximum and minimum in each pixel are needed. For finding the extreme values, random passive phase shifts caused by environmental noises are adopted to make the intensity ergodic. Supplementary active phase shifts, which are not accurately controlled or calibrated, are performed to shorten the measurement cycle. Finally, averaging statistically uncorrelated data over a long enough period of time can effectively reduce most random errors. A minitype Fizeau interferometer applying this random phase-shifting method demonstrated the feasibility of it.

OCIS codes: 120.3180, 120.5050.

Phase-shifting interferometry has been widely used in surface testing of optical elements, especially the large-aperture lens or mirrors in astronomical telescopes or satellite cameras. Owing to the large size of the measured surface, the optical path length is set to be several meters or even longer to complete the testing, and mechanical vibration and air turbulence will change the preset phase shifts and cause inevitable errors to the measurement [1,2]. Dynamic (vibration-insensitive) phase-shifting interferometry has been developed over the years. Phase feedback methods [3,4] with mechanical phase-shifting or acousto-optic modulation can compensate vibrations of small amplitude but suffer from low-contrast interferograms. One-shot or simultaneous phase-shifting interferometers [5,6] succeeded in reducing time-varying noises by capturing the interferograms at the same time with different parts of the same detector. However, complicated phase modulators are needed, and the spatial resolution will be limited with only one detector. Most phase-solving algorithms take the phase shift as a parameter, so they require accurate phase shifts. An antivibration phase-shifting interferometry [7] was developed to use vibration as the only phase shifter to measure large-aperture mirrors. Five frames with the required 90° phase shifts are picked up from a large amount of images for calculation. This method is accurate but very time-consuming (1–2 h for data acquisition) because the vibration is uncontrollable. In this Letter, a random phase-shifting interferometry with both active phase shifts (APSs) and passive phase shifts (PPSs) is proposed. The relationship between intensity and phase in each pixel is obtained from a large amount of phase-shifting interferograms. In the phase-solving algorithm, the temporal intensity maximum and minimum in each pixel are taken as parameters. For finding the extreme values, random PPSs caused by environmental noises and supplementary APSs are adopted to make the intensity ergodic. Finally, averaging statistically uncorrelated data over a long enough time can effectively reduce most random errors, such as air turbulence or measured surface tilt. This random phase-shifting method can be applied to all kinds of surface measurement interferometers.

First, APSs can be simply introduced with mechanical displacement of the measured surface. Suppose N frames of interferograms are collected. According to phase-shifting techniques, the intensity of an arbitrary pixel (x,y) in the ith interferogram is expressed as

$$I(x,y,i) = [I_b(x,y) + I_a(x,y)]\{\cos[\Phi(x,y) + \delta(x,y,i)]\}, \tag{1}$$

where $I_b(x,y)$ and $I_a(x,y)$ present the background intensity and modulation amplitude in pixel (x,y), respectively, $\Phi(x,y)$ is the original phase in pixel (x,y) that is the target of the measurement, and $\delta(x,y,i)$ is the phase shifts for the ith frame; $\delta(x,y,i)$ comprises two parts: APS $\delta_a(i)$ and PPS $\delta_p(x,y,i)$; $\delta_a(i)$ is not accurately controlled or measured but should be the same for all the pixels or, namely, it should be a piston phase shift; $\delta_p(x,y,i)$ is brought in by mechanical vibration, air turbulence, or surface tilt during the movement of the measured surface and may be different from pixel to pixel. In most phase-shifting techniques, $\delta_p(x,y,i)$ should be eliminated with a special algorithm or means, such as feedback or synchronous camera shot, while $\delta_a(i)$ has to be accurately calibrated. However, here the exact phase shift is not used as a parameter for phase-solving. Only the intensity variation is analyzed as follows.

A series of intensity values (or gray scale) in a pixel can be plotted against the frame index as the circle measurement points show in Fig. 1. As long as the phase variation between two adjacent frames, i.e., $\delta(x,y,i+1) - \delta(x,y,i)$, is small enough, the intensity can be ergodic over a long enough time. This requirement can be achieved with a low-speed APS or a high-frequency image sampling. The maximum and the minimum intensity in each pixel, denoted as

0146-9592/09/081288-3/$15.00

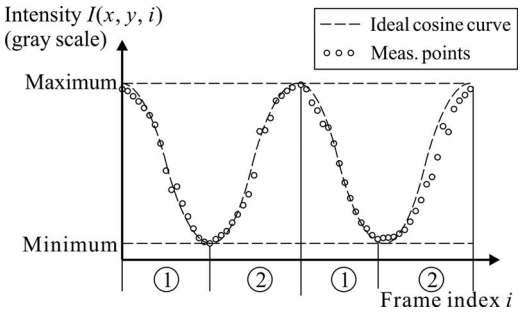

Fig. 1. Intensity curve against the frame index.

$I_{\max}(x,y)$ and $I_{\min}(x,y)$, can be found from the measurement points as they are marked out in Fig. 1. These extreme values are simply related to $I_b(x,y)$ and $I_a(x,y)$ in Eq. (1) as

$$\begin{cases} I_{\max}(x,y) = I_b(x,y) + I_a(x,y) \\ I_{\min}(x,y) = I_b(x,y) - I_a(x,y) \end{cases}. \tag{2}$$

Thus $I_b(x,y)$ and $I_a(x,y)$ in Eq. (1) can be derived from

$$\begin{cases} I_b(x,y) = [I_{\max}(x,y) + I_{\min}(x,y)]/2 \\ I_a(x,y) = [I_{\max}(x,y) - I_{\min}(x,y)]/2 \end{cases}. \tag{3}$$

With $I_b(x,y)$ and $I_a(x,y)$ already known, the total phase in Eq. (1), denoted as $\varphi(x,y,i) = \Phi(x,y) + \delta(x,y,i)$, can be solved from the intensity with arc cosine function,

$$\varphi(x,y,i) = \arccos\left[\frac{I(x,y,i) - I_b(x,y)}{I_a(x,y)}\right]. \tag{4}$$

Since the range of arc cosine function goes from 0 to π, before the unwrapping calculation, it is necessary to recover $\varphi(x,y,i)$ in Eq. (4) to its principal phase in $(0, 2\pi)$. First, the intensity curve is divided into several sections according to the varying trend as shown in Fig. 1. With the $I_{\max}(x,y)$ and $I_{\min}(x,y)$ already known, if a local extreme point in the intensity curve meets some criteria [a simple example: $I(x,y,i) \geqslant 0.9\ I_{\max}(x,y)$], it is denoted as a maximum or minimum point. Then the curve between a maximum (or minimum) point and a minimum (or maximum) point is denoted as section ① (or section ②). Because of environmental noises, especially the vibrations, the intensity curve may have local fluctuations caused by rapid phase changing. The division of different sections will be correct only if the local fluctuation peak or valley does not meet the criteria. As a result high-speed APS is expected so that the amplitude of local fluctuation will be reduced. A compromise between this high-speed requirement and the low-speed requirement aiming for intensity ergodicity should be taken to find a proper APS speed. Then for the measured point in section ①, $\varphi(x,y,i)$ is exactly the principal phase value in (x,y), and for the measured point in section ②, the principal phase value equals $[2\pi - \varphi(x,y,i)]$.

After two-dimensional phase unwrapping in the spatial domain, the unwrapped phase distribution of each interferogram can be obtained from the recovered principal phases. These wavefront distributions may be distorted because of air turbulence and other random factors in image capturing or phase calculation. Consequently, all the N frames of phase maps or wavefront distributions are averaged to get a final measurement result,

$$\varphi'(x,y) = \frac{1}{N}\sum_{i=1}^{N} \mathcal{W}[\varphi(x,y,i)], \tag{5}$$

where $\mathcal{W}$ is a spatial unwrapping operator. In the next part, a detailed analysis on $\varphi'(x,y)$ will be given to further look into the noise insensitive feature of this method.

Since $\varphi(x,y,i)$ comprises three parts, the original phase $\Phi(x,y)$, APS $\delta_a(i)$, and PPS $\delta_p(x,y,i)$, the final result $\varphi'(x,y)$ will reflect these three contributors. In fact, the PPS is mainly caused by mechanical vibration, air turbulence, or surface tilt, and these three error sources performance differently on each pixel. Mechanical vibration phase shift is considered to randomly translate the whole workpiece (WP) or the interferometer, so it is also a piston phase shift and denoted as $\delta_{p1}(i)$. Air turbulence phase shift and surface tilt error phase shift will change the phase locally, and they are expressed by $\delta_{p2}(x,y,i)$. Then $\varphi(x,y,i)$ can be rewritten as

$$\varphi(x,y,i) = \Phi(x,y) + [\delta_a(i) + \delta_{p1}(i)] + \delta_{p2}(x,y,i), \tag{6}$$

where $\Phi(x,y)$ is the target of the measurement and should be dealt with the unwrapping operator. The second term $[\delta_a(i) + \delta_{p1}(i)]$ is the same over the whole aperture and can be taken out from the unwrapping operator. For each pixel, $\delta_{p2}(x,y,i)$ is random in time-domain but small in quantity, so it will not be unwrapped. Because of the above mathematical features of these phase-shifting terms, Eq. (5) can be evolved as

$$\varphi'(x,y) = \mathcal{W}[\Phi(x,y)] + \frac{1}{N}\sum_{i=1}^{N}[\delta_a(i) + \delta_{p1}(i)] + \frac{1}{N}\sum_{i=1}^{N}\delta_{p2}(x,y,i). \tag{7}$$

With a large number of interferograms over a long enough time, the average phase shift caused by air turbulence or surface tilt errors, i.e., the third term, approaches zero. That is why this method is insensitive to local random errors. The second term in Eq. (7) has no relationship with the coordinates of the pixel and thus will not influence the wavefront distribution. The final result $\varphi'(x,y)$ has the same shape with the original phase $\Phi(x,y)$, only with the average piston phase shifts as a bias over the whole aperture.

A minitype interferometer shown in Fig. 2 was built up to demonstrate this method. The Fizeau layout was adopted to save space and reduce errors with common-path settings. The standard plane (nominal $\lambda/20$ over a 20 mm aperture) as well as the image capture system was included in the interferometer

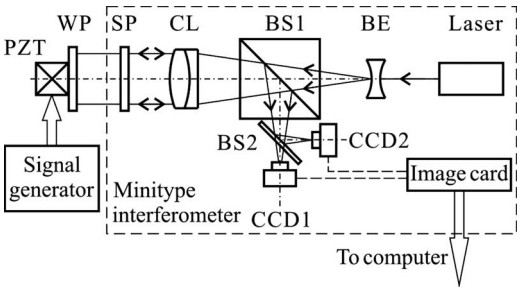

Fig. 2. Configuration of a minitype interferometer adopting the random phase-shifting method. BE, beam expander; BS, beam splitter; CL, collimating lens; SP, standard plane; WP, workpiece; PZT, piezoelectric transducer.

(shown inside the dashed frame). The CCD1 camera was used for interferometer adjustment, and CCD2 records the interferograms. The whole system worked on a common laboratory desk without special vibration isolation or air flow control measures. The APSs were realized with a piezoelectric transducer pushing the WP continuously in a certain direction, and the total APS during the sampling time was about 2π.

A plane WP (nominal $\lambda/10$ over a 20 mm aperture) with an effective aperture of 15 mm was measured with this system; 100 frames of interferograms were captured at a frame frequency of 10 fps. Some typical interferograms are shown in Fig. 3(a) in which the patterns are distorted mainly because of the air turbulence. Owing to the instability in laser energy or random noise in detector, intensity fluctuations can be observed in the experiment even if there is no phase shift. A reference plane is set in the interferometer to pick up intensity fluctuations, and these data are used to do intensity corrections to all the interferograms [8]. After intensity corrections, the time-varying intensity (gray scale) of an arbitrary pixel is plotted in Fig. 3(b). Although there are local fluctuations in the curve, the principal phase recovery can still be done, because the increasing section and the decreasing section are clear. The principal phase of each pixel in each interferogram was solved with the procedure present above, and the Goldstein branch cut algorithm was chosen to perform the phase unwrapping in the spatial domain. The current total time for a measurement cycle was 10 s for data acquisition and 20 min for calculation. The calculation can be accelerated by algorithm optimization. The final wavefront reconstructed from the measurement result is shown in Fig. 3(c) with a peak-to-valley value of 0.027λ, where $\lambda = 632.8$ nm. The repeatability of ten times measurement was 0.004λ. To verify the measurement accuracy, the same plane WP was tested with a Zygo phase-shifting interferometer (GPI XP-IV, 101.6 mm aperture with a repeatability of $\lambda/300$) placed on a vibration isolator. The accuracy

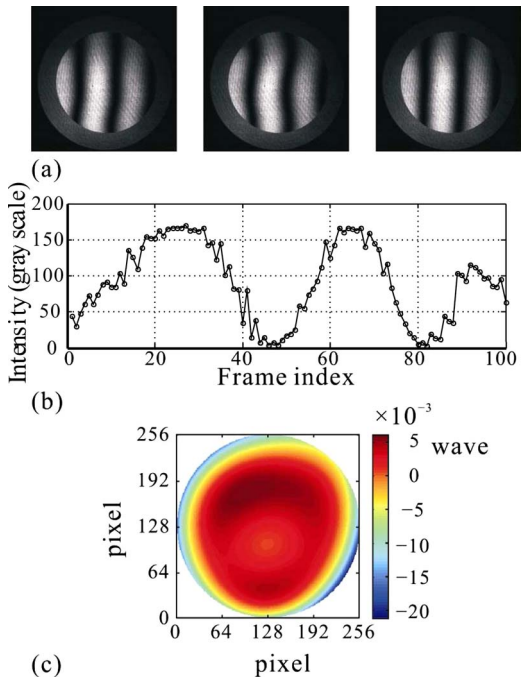

Fig. 3. (Color online) Wavefront measurement result of a plane. (a) Typical interferograms distorted. (b) Gray scale curve against the frame index of an arbitrary pixel. (c) Reconstructed wavefront of the plane.

of the reference optics was $\lambda/20$. A four-step phase-shifting method was used, and the peak-to-valley value was 0.022λ. So the result from our random phase-shifting method coincided well with that from a Zygo interferometer. The minitype interferometer with the new method has the advantages of low cost and relaxed requirements on the phase-shifting accuracy and the environment. The moderate processing speed and noise insensitivity make this method potential for field testing with high accuracy.

This work was supported by the National Natural Science Foundation of China (NSFC) 60578053 and the 111 Project under grant B08043.

References

1. P. DeGroot, Appl. Opt. **34**, 2856 (1995).
2. B. K. A. Ngoi, K. Venkatakrishnan, and N. R. Sivakumar, Appl. Opt. **40**, 3211 (2001).
3. A. A. Freschi and J. Frejlich, Opt. Lett. **20**, 635 (1995).
4. D. Wu, R. Zhu, L. Chen, and J. Li, Optik (Jena) **115**, 343 (2004).
5. G. Rodriguez-Zurita, C. Meneses-Fabian, N. Toto-Arellano, J. F. Vazquez-Castillo, and C. Robledo-Sanchez, Opt. Express **16**, 7806 (2008).
6. M. Novak, J. Millerd, N. Brock, M. North-Morris, J. Hayes, and J. Wyant, Appl. Opt. **44**, 6861 (2005).
7. J. Hayes, Laser Focus World **38**, 109 (2002).
8. Q. Hao, Q. Zhu, Y. Hu, and L. Tang, Chinese patent application 200810188355.2 (filed Dec. 25, 2008).